A Three-Dimensional Quantitative Structure−Activity Relationship Study of Heparin-Binding Epidermal Growth Factor Shedding Inhibitors Using Comparative Molecular Field Analysis

Roberta Bursi,*[,†] Masaaki Sawa,[‡,§] Yasuyuki Hiramatsu,[‡,#] and Hirosato Kondo[‡,⊥]

Department of Molecular Design & Informatics, N.V.Organon, P.O. Box 20, 5340 BH Oss, The Netherlands, and Department of Chemistry, R&D Laboratories, Nippon Organon K.K., 1-5-90, Tomobuchi-cho, Miyakojima-ku, Osaka 534-0016, Japan

Received September 7, 2001

Despite the lack of structural information on the heparin-binding (HB) epidermal growth factor (EGF) shedding putative target enzyme, the design of potent HB-EGF shedding inhibitors has been attempted by means of comparative molecular field analysis (CoMFA), a well-established 3D-QSAR technique. Two different binding modes, obtained by docking a flexible representative into the MMP-3 and TACE target enzymes, were considered as alignment rules for an in-house data set of 50 HB-EGF shedding inhibitors. CoMFA models were derived with the standard steric, electrostatic, and Bohacek and McMartin's H-bond molecular fields. These fields were used individually or in combination. For both alignments, the H-bond field alone yielded the best statistical models. From the analysis of the CoMFA contours, ideas for testing the size of the S1′ pocket and suggestions for the design of new inhibitors came forward, resulting in the synthesis and testing of four new inhibitors. Three of four compounds turned out to possess from good (IC_{50} = 0.56 and 0.60 μM) to excellent (IC_{50} = 0.13 μM) inhibitory activity. The hypothesis that, upon binding, the S1′ pocket in the vicinity of the R^1 benzene ring must be narrow in size was confirmed by the weak activity (IC_{50} = 1.1 μM) of the fourth compound. The experimental profile of these new inhibitors does suggest the MMP-3 alignment as the most plausible one for HB-EGF shedding inhibitors.

Introduction

Heparin-binding (HB) epidermal growth factor (EGF)-like growth factor is a member of the EGF family that stimulates growth and differentiation.[1,2] HB-EGF is synthesized as a membrane-anchored precursor (proHB-EGF), and then mature HB-EGF is released from the cell surface by regulated proteolytic processing as other transmembrane proteins.[3] The importance of such transmembrane protein shedding for cytokine biology has been increasingly recognized.[4] HB-EGF has been implicated as a participant in a variety of normal and aberrant processes such as wound healing, blastocyst implantation, SMC hyperplasia, atherosclerosis, and tumor growth.[5] Thus, agents, which inhibit HB-EGF production, would be effective in the treatment of such diseases.

To our knowledge, the responsible enzyme for HB-EGF shedding has not been identified as yet, and no structure−activity relationship (SAR) studies on HB-EGF shedding inhibitors have been reported in the literature. Several studies, however, have suggested that zinc-dependent metalloproteases are involved in the processing of proHB-EGF.[6,7] The active site of the putative enzyme seems to be very similar to the active site of other zinc-dependent metalloproteases, such as the matrix metalloproteinases (MMPs), since several MMP inhibitors blocked the phorbol ester 12-*O*-tetradecanoylphorbol-13-acetate (TPA) induced HB-EGF secretion.

The rational design of new HB-EGF shedding inhibitors is strongly disturbed by a lack of structural information on the responsible target enzyme. For this reason, we have reported the SAR of a series of non-peptidic hydroxamate-based bicyclic derivatives as inhibitors of HB-EGF shedding to obtain a better understanding of the SAR of the responsible enzyme.[8−10]

Nowadays, a 3D quantitative structure−activity relationship (3D-QSAR)[11−13] technique such as Comparative Molecular Field Analysis (CoMFA)[14] is routinely used in structure-based drug design to obtain topological information on the active site of the investigated target in terms of molecular fields (mostly steric and electrostatic) complementarity. It has been already shown in the literature that this approach can strongly support and help the design of novel and potent inhibitors.[15−19] In this study, a CoMFA analysis of a in-house series of HB-EGF shedding inhibitors was performed, and the active site's topographical features of the putative sheddase were discussed. Moreover, we designed and synthesized new inhibitors based on the CoMFA results and tested their *in vitro* efficacy.

Methods

Chemistry. The structures of the 50 compounds used in this study are listed in Tables 1 and 2. These compounds have

* To whom correspondence should be addressed. Tel: (+31) (0)412-661468. Fax: (+31) (0)412-662539. E-mail: roberta.buma@organon.com.
† N.V.Organon.
‡ Nippon Organon K.K.
§ New address: Chemistry Research Laboratories, Drug Research Division, Dainippon Pharmaceutical Co., Ltd., Osaka 564-0053, Japan.
# New address: Medicinal Chemistry, Discovery Research Laboratories, Shionogi & Co., Ltd., Osaka 553-0002, Japan.
⊥ New address: Manufacturing Technology R & D Laboratories, Shionogi & Co., Ltd., Hyogo 660-0813, Japan.

10.1021/jm0110385 CCC: $22.00
Published on Web 01/18/2002

Table 1. Chemical Structures and HB-EGF Shedding Inhibition Data of 1,2,3,4-Tetrahydroisoquinoline Derivatives

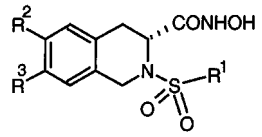

compd	R^1	R^2	R^3	HB-EGF shedding IC_{50} (μM)
1		-H	-H	0.28
2		-H	-H	1.1
3		-H	-H	0.83
4		-H	-H	0.042
5		-H	-H	0.34
6		-H	-H	5.5
7	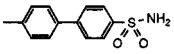	-H	-H	20
8		-H	$-NH_2$	0.19
9		-H		0.28
10	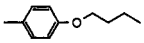	-H	-H	0.42
11		-H	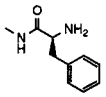	0.57
12		-H		0.36
13	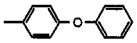	-H	$-NH_2$	0.49
14	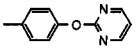	-H	$-NH_2$	4.5
15	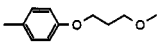	-H	$-NH_2$	0.039
16		-OH	-OH	0.73
17	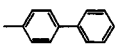	-OH	-OH	1.29
18		-OH	-OH	0.16
19	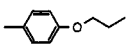	-OH	-OH	0.63
20	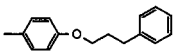	-OH	-OH	0.99
21	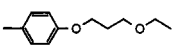	-OH	-OH	0.21
22	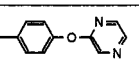	-OH	-OH	0.82
23		-OH	-OH	5.40

been synthesized from sulfonyl chlorides and 1,2,3,4-tetrahydroisoquinoline derivatives or 5,6,7,8-tetrahydropyrido[3,4-*b*]-pyrazine derivatives as described in the patent and elsewhere (Scheme 1).[8,9] Thus, 1,2,3,4-tetrahydroisoquinoline derivatives or 5,6,7,8-tetrahydropyrido[3,4-*b*]pyrazine derivatives were treated with appropriate sulfonyl chlorides (commercially available or prepared from corresponding sulfonic acids with thionyl chloride or corresponding aromatic compounds with

Table 2. Chemical Structures and HB-EGF Shedding Inhibition Data of 5,6,7,8-Tetrahydropyridopyrazine Derivatives

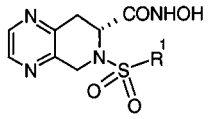

compd	R^1	HB-EGF shedding IC_{50} (μM)
24	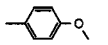	0.35
25	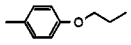	1.0
26	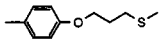	0.10
27	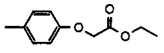	1.0
28		2.7
29	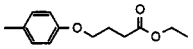	1.1
30	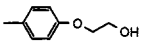	1.5
31		4.4
32	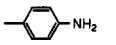	1.8
33		6.9
34	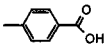	70
35	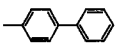	1.5
36		12
37	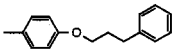	0.63

compd	R^1	HB-EGF shedding IC_{50} (μM)
38		0.96
39		40
40	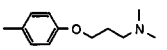	18
41		70
42	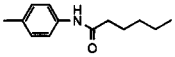	7.7
43	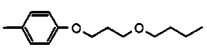	0.26
44	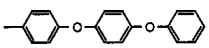	6.1
45	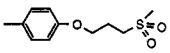	1.8
46	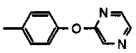	0.11
47	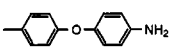	1.0
48	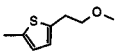	3.0
49	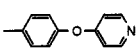	0.34
50	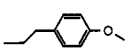	6.7

Scheme 1

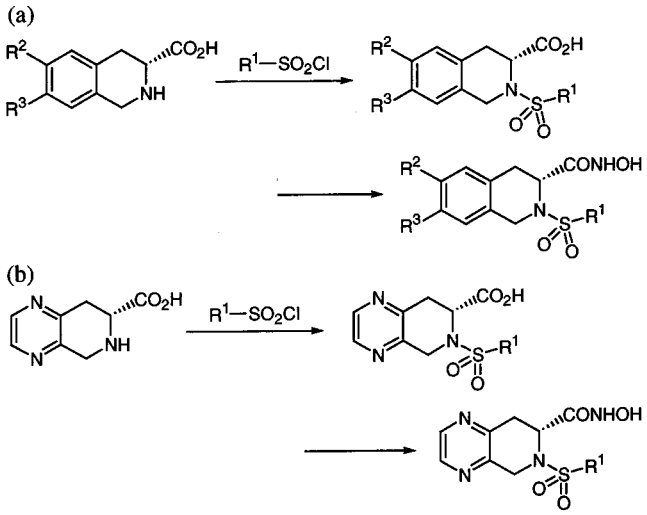

chlorosulfonic acid) in dioxane−water in the presence of organic bases. In the case of the 6,7-dihydroxyl analogue, the reaction was carried out in the presence of sodium tetraborate and sodium hydroxide to protect hydroxyl groups. The resulting sulfonamides were converted to the corresponding hydroxamic acids by commonly used procedures. All compounds gave characteristic data (^{1}H NMR, MS spectra, and combustion analyses) that fulfilled Organon criteria (purity ≥ 95%) for biological testing.

HB-EGF Shedding Inhibition Assay.[7] Fibrosarcoma HT-1080 transfectants expressing human placental alkaline phosphatase (AP)-tagged HB-EGF in MEM (containing 10% FCS) as culture medium were seeded in 96-well plates at a density of 2×10^5 cells/well and incubated for 24 h. The cells were washed with PBS and preincubated with the test compounds in MEM (containing 1% DMSO) for 30 min. TPA (60 nM) was added to stimulate inducible processing, and the plate was incubated for 60 min. A 0.1 mL aliquot of the supernatant was transferred to a 96-well plate and heated for 10 min at 65 °C in order to inactivate endogenous alkaline phosphatases. A 0.1 mL of substrate solution (1 M diethanolamine, 0.01% $MgCl_2$, 1 mg/mL *p*-nitrophenyl phosphate, pH 9.8) was added to each well, and the plate was incubated for 2 h. AP activity was then determined by the measurement of absorbance at 405 nm with a microplate reader. The IC_{50} values were determined with different inhibitor concentrations by using GraphPad Prism Version 3.0 (GraphPad Software, Inc.).

Computational Procedures. Within CoMFA, structural superposition is a *condicio sine qua non*. Structures must be aligned with respect to a reference compound or template, which mimics the binding mode of the investigated compounds with respect to their corresponding target. When experimental information is available, CoMFA potential is maximized. In absence of such information, structural alignment can become

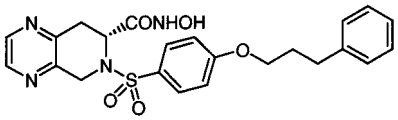

Figure 1. Two-dimensional structure of compound **37**.

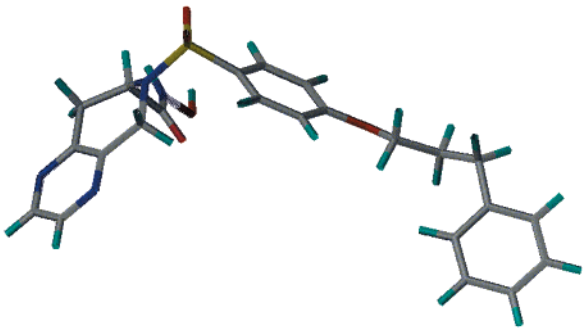

Figure 2. Conformation of **37**-MMP.

a problem, particularly when flexible compounds need to be superimposed.

As can be seen in Tables 1 and 2, in most of the HB-EGF inhibitors present in our data set the R^1 substituents on the sulfonamide moiety are *p*-substituted phenyl rings and these *para* substituents are quite flexible. In few inhibitors, *o*- or *m*-substitutions come forward as well, and their orientation with respect to the sulfonamide-bridging moiety is clearly a critical issue. Further, R^1 substituents are not only (un)-substituted phenyl moieties but also include heterocycles, like (un)substituted thiophens or pyridines. The position of the heteroatom with respect to the sulfonamide bridge is also critical.

Since meaningful CoMFA models could only be produced when all these issues were properly dealt with, modeling work was performed in order to explore all alignment possibilities and to arrive at (a) highly probable binding mode(s) of these inhibitors toward their putative enzyme. The computational strategy, which was followed in this study, is explained below.

Calculation of the Expected Bioactive Conformation-(s) of Flexible Inhibitors. Compound **37** (Figure 1) was chosen as a typical flexible representative of this data set. A docking study was then performed on both the MMP-3 (bis-sulfonamide inhibitor complex, PDB code: 1BQO)[20] and TACE (peptide-based inhibitor complex, PDB code: 1BKC).[21] These enzymes were chosen as target enzymes since the inhibition profiles of our compounds on MMP-3, TACE, and HB-EGF shedding look similar.[10]

Compound **37** was manually docked into the active sites of these enzymes. First, compound **37** was placed in the active site of the MMP-3 to occupy the S1′ pocket with the R^1 group. Then, the sulfonamide moiety of compound **37** was superimposed on one of the sulfonamide moieties of the bis-sulfonamide inhibitor. Then, the protein−ligand complexes were energy minimized, treating all ligand atoms and retaining all protein atoms. Next, the MMP-3/compound **37** complex model was superimposed on TACE/peptide-based inhibitor complex to overlap the C-α chains of the enzymes. Then, the peptide-based inhibitor was replaced by compound **37**, and the obtained protein−ligand complexes were subsequently energy minimized, treating all ligand atoms and retaining all protein atoms. This led to two possible conformations of compound **37**, the **37**-MMP and the **37**-TACE conformation, respectively. These are shown in Figures 2 and 3. Docking and energy minimizations were performed with the TRIPOS force field[22] within the SYBYL program.[23] All computations were performed on an Octane Silicon Graphics workstation.

Calculation of the Expected Directions of *o*-, *m*-Substituents at the Phenyl Ring or the Sulfur/Nitrogen Atom in the Thiophen/Pyridine Ring Attached to the Sulfonamide. Compounds **36**, **51**, **38**, and **33** (see Figure 4) were chosen as representatives of *o*-, *m*-substituted phenyl and

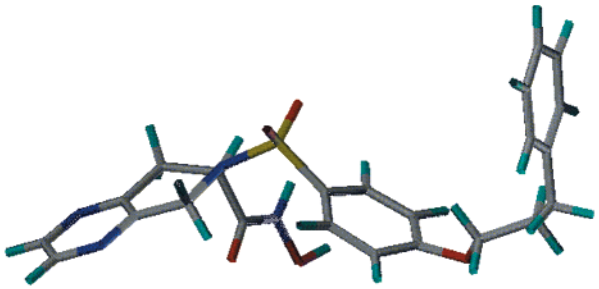

Figure 3. Conformation of **37**-TACE.

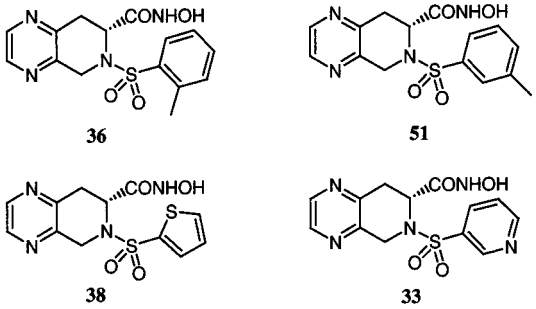

Figure 4. Compounds chosen as representatives of *o*-, *m*-substituted phenyl and thiophen/pyridin R1 substituents of the sulfonamide.

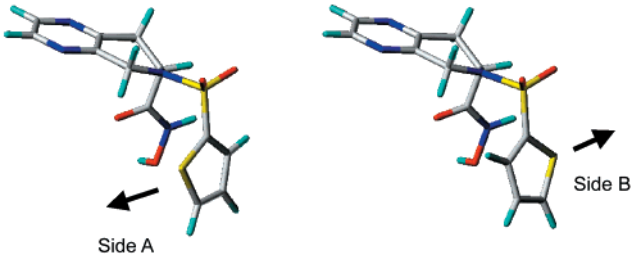

Figure 5. Orientation of sides A and B, respectively.

Table 3. Comparison of the Energy Differences of the Protein−Ligand Complexes

	MMP-3	TACE
compd	energy difference ($A - B$) kcal/mol	energy difference ($A - B$) kcal/mol
38	1.0	−1.6
51	−4.0	5.8
36	−2.5	−3.6
33	−1.5	−2.3

thiophen/pyridine R^1 substituents of the sulfonamide. These four compounds were docked in their two possible corresponding conformations, which we will call here for simplicity "side A" and "side B", into the active sites of MMP-3 and TACE (see Figure 5). The eight complexes were energy minimized (by always keeping the structure of the protein rigid), and the energy differences between side A and side B were obtained. The results are shown in Table 3. Since three of four complexes possess the lowest energy when the ligand is present in the conformation pointing to side A in both MMP-3 and TACE active sites, we have chosen side A as alignment orientation of this subgroup of inhibitors. Docking and energy minimizations were performed with the SYBYL program.

CoMFA Models Development. The remaining data set was energy minimized, and Coulson partial charges were calculated at the AM1 semiempirical level[24] for all compounds. The data set was then aligned on each of the two templates, **37**-MMP and **37**-TACE, in two steps: first, a rigid alignment was performed on the tetrahydropyridopyrazine and the sulfonamide moieties; second, the flexible substituents of the phenyl ring in R^1 moieties were aligned by flexible fitting to

match the orientation of the phenylpropoxy substituent of **37**-MMP and **37**-TACE, respectively. CoMFA models were derived on the two resulting data sets.

SYBYL standard steric (van der Waals radii), electrostatic (Coulson partial charges), and H-bond[25,26] fields were applied. The H-bond field is based on the Lee and Richards accessible surface (L&R surface), which consists of a van der Waals radius plus a probe radius away from the ligand. In Bohacek's study, it was shown that this surface can display regions for hydrophobic, hydrogen-bond acceptor, and hydrogen-bond donor properties around the ligand, which are accurate and complementary to the target protein. Regions on the protein surface where hydrogen bonds can be formed can be expected to be hydrophilic, while regions which lack hydrogen-bonding groups are likely to be hydrophobic. Further, the H-bond field has an advantage on the electrostatic calculation, since it is not force field dependent while atomic partial charges are.

Within CoMFA, the H-bond field has been implemented in an acceptor ("steric" field type) and a donor ("electrostatic" field type) component, as given by Bohacek and McMartin. The green and yellow contours will therefore display the favorable and unfavorable acceptor field-type regions, while the red and blue contours will display the favorable and unfavorable donor field-type regions.

Field values were not smoothed, and the cutoff values of steric and electrostatic interactions were kept to the default values of 30.0 kcal/mol. A smooth transition was chosen between the cutoff plateaus for the steric and the electrostatic calculations, and every Coulombic electrostatic energy calculation was performed using a distance-dependent dieletric $\epsilon = R$. The CoMFA standard scaling procedure was used throughout the analyses.

Performing the CoMFA analyses at 1 Å grid distance ensured rotational and translational invariance of the statistical results (q^2 and r^2). Cross-validated correlation coefficients, q^2, were obtained with SAMPLS,[27] and subsequent final correlation coefficients, r^2, were calculated with conventional PLS.[28] In every analysis, the standard error of estimate, s, associated with both q^2 and r^2 is provided as well as the F-ratio, which is the ratio between r^2 and $1 - r^2$ (explained to unexplained). The larger is the F-ratio, the better is the model.

Correlation chances were checked repeatedly by performing PLS analyses on randomized activity ($-\log IC_{50}$ (μM)) sets. No "randomized" models turned out to have cross-validated correlation coefficient values, q^2, close to the correct one.

Results and Discussion

CoMFA Models. Several models were derived by applying steric, electrostatic, and H-bond fields individually and in combination. In Table 4, the results for the **37**-MMP alignment are shown. Clear differences were found between cross-validated correlation coefficients (q^2) and the number of latent variable (LV) values obtained at 2 (default) and 1 Å grid distances for each analysis, suggesting some grid dependence of the statistical results. We will focus therefore our attention only on the results obtained at the highest resolution (1 Å). When molecular fields were used individually, the H-bond field resulted to be the best ($q^2 = 0.41$, $s = 0.61$, 4 LV, $r^2 = 0.90$, $s = 0.25$), followed by the steric field ($q^2 = 0.35$, $s = 0.64$, 5 LV, $r^2 = 0.87$, $s = 0.29$). The electric field alone did not provide an acceptable model. This result was quite surprising since in most compounds, although quite hydrophobic in nature, large polar substituents are present. When molecular fields were combined, the addition of the electrostatic field to the steric or the H-bond field did not improve the statistics of the corresponding individual models. In the particular combination of the electrostatic and the H-bond field, the result is poor.

Table 4. CoMFA Models Based on the **37**-MMP Alignment[a]

field(s)	grid (Å)	q^2	s	# LV	r^2	s	F	field %
ster	2	0.15	0.71	1	0.38	0.60	29.4	
ster	1	0.35	0.64	5	0.87	0.29	59.8	ster (1.00)
elec	2	0.30	0.66	4	0.83	0.33	65.6	
elec	1	0.21	0.68	1	0.42	0.58	35.2	elec (1.00)
H-bond	2	0.16	0.72	3	0.70	0.43	36.3	
H-bond	1	0.41	0.61	4	0.90	0.25	98.4	acc (0.56)/ don (0.44)
ster + elec	2	0.37	0.63	5	0.91	0.25	83.5	
ster + elec	1	0.37	0.63	4	0.89	0.26	89.9	ster (0.46)/ elec (0.54)
ster + H-bond	2	0.23	0.68	2	0.69	0.44	51.2	
ster + H-bond	1	0.45	0.59	5	0.95	0.18	162.3	ster (0.22)/ acc (0.42)/ don (0.36)
elec + H-bond	2	0.21	0.70	3	0.75	0.39	46.6	
elec + H-bond	1	0.34	0.63	2	0.77	0.37	79.5	elec (0.24)/ acc (0.40)/ don (0.36)
ster + elec + H-bond	2	0.22	0.68	2	0.69	0.43	51.8	
ster + elec + H-bond	1	0.43	0.61	5	0.95	0.18	158.6	ster (0.18)/ elec (0.18)/ acc (0.34)/ don (0.30)

[a] Molecular fields were calculated at 2 (default) and 1 Å grid distances, respectively. AM1 semiempirical charges were employed to account for electrostatic interactions. The H-bond field is described in terms of H-bond acceptor and donor components.

This might well be due to an intrinsic correlation between these fields. The combination of the steric and the H-bond fields, on the contrary, resulted in some, although limited, improvement of the corresponding individual models. To a certain extent, this result was disappointing since more was expected from the combination of two fields, which, if taken alone, well describe this data set. Plausible conclusion of this result is that, as for the electrostatics counterpart, the H-bond field based on the L&R accessible surface is correlated to a certain extent to the steric field. When all three molecular fields were employed, no significant statistical improvements were obtained.

In the last column on the right-hand side of Table 4, field contributions to each analysis are displayed. From these values, it can be clearly seen that the H-bond field accounts for the largest model contributions when it is combined either with the steric or the electrostatic fields. In the three-fields combination, the H-bond field is still the major contribuent (64%) to the model.

In conclusion, two statistically significant models were obtained for the **37**-MMP alignment: the H-bond field alone and in combination with the steric field. Since the latter provides slightly better statistics (q^2 and s values) than the former, but with the requirement of an extra component (5 LV against 4 LV), the H-bond field alone was preferred to the combination and was called model 1.

The results of the CoMFA models based on the **37**-TACE alignment are shown in Table 5. In this case, no significant differences were found between the models obtained at 2 or 1 Å grid distances. For consistency, however, with the former analysis, we will focus our attention again on the highest resolution models. While looking at the results, one can see that these models, on average, required a smaller number of components with respect to their corresponding models shown in Table 4. This generally caused smaller final correlation

Table 5. CoMFA Models Based on the **37**-TACE Alignment[a]

field(s)	grid (Å)	q^2	s	# LV	r^2	s	F	field %
ster	2	0.27	0.66	2	0.55	0.52	28.5	
ster	1	0.35	0.63	3	0.74	0.40	44.5	ster (1.00)
elec	2	0.18	0.69	1	0.36	0.61	27.2	
elec	1	0.20	0.69	1	0.38	0.60	29.8	elec (1.00)
H-bond	2	0.42	0.59	3	0.79	0.36	59.2	
H-bond	1	0.42	0.60	3	0.82	0.34	67.6	acc (0.59)/ don (0.41)
ster + elec	2	0.25	0.66	1	0.44	0.57	38.0	
ster + elec	1	0.28	0.66	2	0.70	0.43	53.8	ster (0.49)/ elec (0.51)
ster + H-bond	2	0.40	0.60	2	0.73	0.40	64.7	
ster + H-bond	1	0.38	0.61	2	0.73	0.40	65.9	ster (0.28)/ acc (0.39)/ don (0.33)
elec + H-bond	2	0.38	0.62	3	0.82	0.34	67.4	
elec + Hbond	1	0.37	0.62	3	0.83	0.32	74.9	elec (0.24)/ acc (0.43)/ don (0.33)
ster + elec + H-bond	2	0.37	0.62	2	0.73	0.40	63.1	
ster + elec + H-bond	1	0.35	0.63	2	0.73	0.41	62.0	ster (0.23)/ elec (0.17)/ acc (0.32)/ don (0.28)

[a] Molecular fields were calculated at 2 (default) and 1 Å grid distances, respectively. AM1 semiempirical charges were employed to account for electrostatic interactions. The H-bond field is described in terms of H-bond acceptor and donor components.

coefficients values (r^2). Despite these differences, it can be concluded that the general statistical trend that was identified in the models based on the **37**-MMP alignment comes forward in these models as well.

The best model was obtained with the H-bond field alone ($q^2 = 0.42$, $s = 0.60$, 3 LV, $r^2 = 0.82$, $s = 0.34$), while the poorest one was again the electrostatic field. The H-bond field was called model 2. Within the framework of this alignment, no field combination yield statistically improved models, and the individual field contributions are comparable to the ones given in Table 4.

CoMFA Contours. In absence of information on the experimental binding mode of these compounds toward their putative target enzyme, one could be tempted of identifying such binding mode in the alignment, which has produced the best statistical results. Unfortunately, this may not be the case. We have previously discussed[29] that better statistical results do not necessarily point to the actual binding mechanism and that in some cases experimental alignments can lead to worse statistics than *a priori*, theoretically derived, and nonphysical structural superpositions. For this reason, we regarded models 1 and 2 as equally plausible, and we proceeded to analyze the molecular field contours of both.

The H-bond contours of model 1 are displayed in Figure 6. While looking at these contours, it must be borne in mind that the acceptor component contributions of the H-bond field are depicted in green (favorable) and yellow (unfavorable), while the donor component contributions are given in red (favorable) and blue (unfavorable). The model provides major information mostly around the hydroxamic acid substituent on the tetrahydropyridopyrazine and around the R^1 flexible substituent (S1′ pocket) covering approximately a 6 Å distance from the benzene ring.

In the first case, the region around the hydroxamic acid group is described by both donor and acceptor H-bond field components, the donor component being the most important one. Clearly, the presence of H-bond donating and accepting groups at this site of the inhibitors is very important for the desired activity profile. At the same time, these contours suggest a highly hydrophilic region at the complementary site of the putative enzyme-binding pocket.

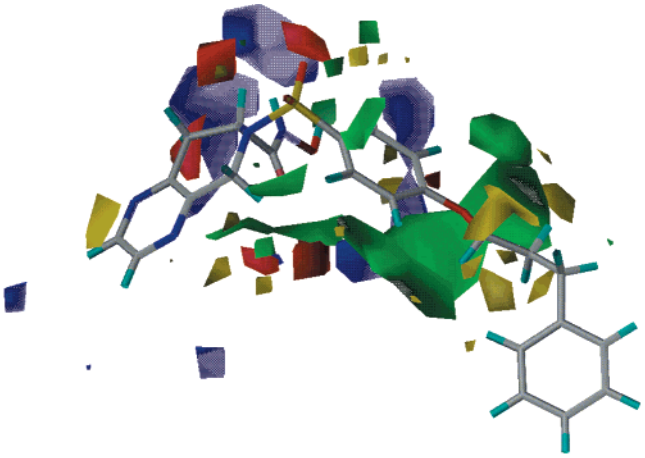

Figure 6. CoMFA contours of model 1, **37**-MMP. The green and yellow contours display favorable and unfavorable H-bond acceptor field-type regions, while the red and blue contours display the favorable and unfavorable H-bond donor field-type regions, respectively.

In the second case, only the acceptor component is present, and the green and yellow regions are present almost 360° all around the flexible chains, the green regions being the closest ones to the substituent. The analysis shows that the presence of acceptor group(s) in this region of the S1′ pocket will indeed increase the affinity of the inhibitors, but that these groups may not be large in size. This result suggests that a hydrophilic region (H-bond donors) must be present in the corresponding site of the putative enzyme, but that the available space in the cavity upon binding must be quite narrow.

Further, minor H-bond field contributions are present at the very end of the S1/S2 pocket alongside the tetrahydropyridopyrazine moiety and below the tetrahydropyridopyrazine plane at several ångströms of distance. Few small field contributions are also present around the sulfonic bridge. No H-bond field contributions were found above the tetrahydropyridopyrazine plane, suggesting that this region must be hydrophobic in nature. This result agrees with the description of the S1/S2 sites in both MMP-3 and TACE,[15] where a π-stacking interaction is envisaged between ligand and enzyme.

Finally, no H-bond contributions are present at the very end of the flexible R^1 substituents, suggesting the presence of a region in the ligands (and therefore in the enzyme), where hydrophobic interactions prevail.

The H-bond contours of model 2 are displayed in Figure 7. Bearing in mind the results that were just discussed for model 1, it was interesting to see that similar information could be extracted from the contours of model 2 despite the completely different orientation of the flexible chains of the R^1 substituents.

The only differences are some larger donor contours alongside the tetrahydropyridopyrazine moiety at the very end of the S1/S2 pocket and the presence of a small donor contour in the S1′ pocket.

Table 6. Chemical Structures and HB-EGF Shedding Inhibition Data of 5,6,7,8-Tetrahydropyridopyrazine Derivatives, CoMFA Predictions, and Percentage Error ($Y_{Exp} - Y_{Pred}/Y_{Exp}$)

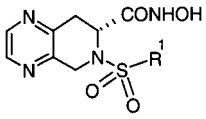

compd	R^1	HB-EGF shedding IC_{50} (μM)	HB-EGF shedding -Log(IC_{50})	model 1 -Log(IC_{50}) (Error%)	model 2 -Log(IC_{50}) (Error%)
52	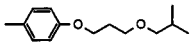	0.56	6.25	6.14 (1.8%)	5.85 (6.4%)
53	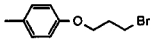	0.60	6.22	6.00 (3.5%)	6.40 (3.2%)
54	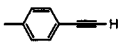	0.13	6.89	6.15 (10.7%)	5.93 (13.9%)
55		1.1	5.96	5.85 (1.9%)	6.03 (1.2%)

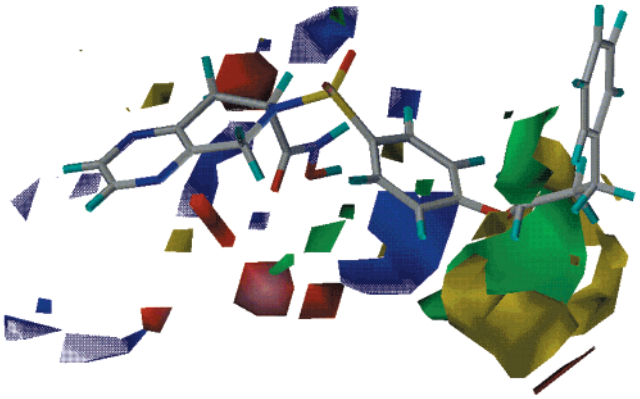

Figure 7. CoMFA contours of model 2, **37**-TACE. The green and yellow contours display favorable and unfavorable H-bond acceptor field-type regions, while the red and blue contours display the favorable and unfavorable H-bond donor field-type regions, respectively.

By the analyses of the contours of models 1 and 2, it could be concluded that for this data set of inhibitors both alignments tend to provide similar information on the binding cavity of the HB-EGF putative target enzyme.

Evaluation of New Inhibitors. The CoMFA models 1 and 2 were applied to the design of new HB-EGF shedding inhibitors.

If we look at the S1′ pocket, according to these models the addition of groups to the end of the alkoxyphenyl moiety may increase the activity as long as these groups are narrow and polar (H-bond acceptors) in the vicinity of such moiety and bulky and hydrophobic at the very end. By making use of this information and checking upon synthetic feasibility, four new inhibitors (see Table 6) were designed with the following strategy: two compounds (**52** and **53)** were designed with a narrow and polar (H-bond acceptors) long tail. In one of the two, compound **52**, a bulky and hydrophobic substituent was added at the very end of the tail. Two compounds (**54** and **55**) were designed with short and polar (high electron density) tails. In compound **54**, the acetylene moiety was expected to well fit the narrow space present in the cavity upon binding in the vicinity of the phenyl group. In compound **55**, the ethylene group was *ad hoc* chosen to test the actual available space of this narrow site, and it was expected to be potentially less active because of its bending shape.

The 5,6,7,8-tetrahydropyrido[3,4-*b*]pyrazine scaffold was chosen as mother skeleton in all four compounds in order to compensate for potential hydrophobicity of the new substituents.[8]

In silico predictions, synthesis, and testing were performed on these four compounds. Computational and experimental results are shown in Table 6. Compounds **52** and **53** exhibited excellent inhibitory activity against HB-EGF shedding with sub-micromolar IC_{50} values, although their activity was slightly less than the corresponding parent compound **24**. Compound **54** exhibited excellent inhibitory activity against HB-EGF shedding ($IC_{50} = 0.13$ μM), which places it among the most potent inhibitors of the in-house data set considered here, while the activity of compound **55** showed moderate activity as expected ($IC_{50} = 1.1$ μM). Both CoMFA models 1 and 2 turned out to have well predicted three of the four compounds, as the error percentages show. Interestingly, both models had underestimated compound **54**. An important difference, however, between the two models needs to be outlined: while model 1 did predict semiquantitatively the experimental trend and, in particular, the relative activities of compounds **54** and **55**, model 2 did not. Although limited to a small set of compounds, these results seem to point at model 1 as the model, which better describes the most probable binding mode of these HB-EGF shedding inhibitors.

Conclusions

At present, the design of potent HB-EGF shedding inhibitors as well as the identification of the HB-EGF shedding putative target enzyme are great challenges for many scientists at universities and pharmaceutical companies.

In this study, we have attempted the design of new and potent compounds by means of performing comparative molecular field analysis on an in-house congeneric data set of HB-EGF shedding inhibitors.

Plausible alignment rules were derived from structural information provided by the MMP-3 and TACE

complexes, leading to two possible hypothetical binding modes of our flexible inhibitors in the putative binding cavity of the HB-EGF shedding target enzyme.

CoMFA models were subsequently obtained with different molecular fields. Surprisingly, most models showed modest cross-validated correlation coefficients ($q^2 < 0.4$), despite the high degree of relation of the inhibitors considered. The H-bond molecular field did not only yield the best statistical models for both alignments, but it also provided a simple and intuitive description of the structure−activity relationship of these compounds in terms of H-bond acceptor/donor contributions and complementary hydrophobicity.

From considerations based on synthetic feasibility and CoMFA analyses and contours, novel inhibitors were designed, synthesized, and tested for model validation. The experimental results did confirm both models as predictive, did unravel three new compounds with excellent HB-EGF shedding inhibitory activity, and did suggest for these inhibitors the MMP-3-based alignment as the most probable one.

Despite the complexity of the objective before us, the necessary assumptions, and the intrinsic limitations of the techniques to our disposal, this study confirmed the utility of CoMFA in particular and rational drug design in general to set steps forward in this specific area of research.

Acknowledgment. We greatly acknowledge Dr. S. Higashiyama (School of Medicine, Osaka University, Osaka, Japan) for the gift of the expression vector of HB-EGF fused with human placental alkaline phosphatase (AP) and Dr. J. de Vlieg (Molecular Design & Informatics) for support during the preparation of this manuscript.

References

(1) Higashiyama, S.; Abraham, J. A.; Miller, J.; Fiddes, J. C.; Klagsbrun, M. A Heparin-Binding Growth Factor Secreted by Macrophage-Like Cells that is Related to EGF. *Science* **1991**, *251*, 936−939.

(2) Hashimoto, K.; Higashiyama, S.; Asada, H.; Hashimura, E.; Kobayashi, T.; Sudo, K.; Nakagawa, T.; Damm, D.; Yoshikawa, K.; Taniguchi, N. Heparin-binding Epidermal Growth Factor-like Growth Factor is an Autocrine Growth Factor for Human Keratinocytes. *J. Biol. Chem.* **1994**, *269*, 20060−20066.

(3) Piepkorn, M.; Pittelkow, M. R.; Cook, P. W. Autocrine Regulation of Keratinocytes: The Emerging Role of Heparin-binding, Epidermal Growth Factor-related Growth Factors. *J. Invest. Dermatol.* **1998**, *111*, 715−721.

(4) Müllberg, J.; Althoff, K.; Jostock, T.; Rose-John, S. The Importance of Shedding of Membrane Proteins for Cytokine Biology. *Eur. Cytokine Network* **2000**, *11*, 27−37.

(5) Raab, G.; Klagsbrun, M. Heparin-binding EGF-like Growth Factor. *Biochim. Biophys. Acta* **1997**, *1333*, F179−F199. A review.

(6) Prenzel, N.; Zwick, E.; Daub, H.; Leserer, M.; Abraham, R.; Wallasch, C.; Ullrich A. EGF Receptor Transactivation by G-protein-coupled Receptors Requires Metalloproteinases Cleavage of proHB-EGF. *Nature* **1999**, *402*, 884−888.

(7) Tokumaru, S.; Higashiyama, S.; Endo, T.; Nakagawa, T.; Miyagawa, J.; Yamamori, K.; Hanakawa, Y.; Ohmoto, H.; Yoshino, K.; Shirakata, Y.; Matsuzawa, Y.; Hashimoto, K.; Taniguchi, N. Ectodomain Shedding of Epidermal Growth Factor Receptor Ligands is Required for Keratinocyte Migration in Cutaneous Wound Healing. *J. Cell. Biol.* **2000**, *151*, 209−219.

(8) Yoshiizumi, K.; Yamamoto, M.; Miyasaka, T.; Ito, Y.; Kumihara, H.; Sawa, M.; Kiyoi, T.; Yamamoto, T.; *et al.* Synthesis, HB-EGF Shedding Inhibitory Activities and MMP Inhibitory Activities of Hydroxamic Acids Having Pyrido[3,4-*b*]pyrazine Skeleton. Submitted for publication.

(9) Hashimoto, J.; Higashiyama, S.; Yoshino, K.; Yoshiizumi, K.; Yamamoto, M.; Kiyoi, T.; Kurokawa, K.; Kondo, H.; Sawa, M.; Kumihara, H. Keratinocyte Growth Inhibitors and Hydroxamic Acid Derivatives. PCT Patent Application. WO 01/70269.

(10) Sawa, M.; Kiyoi, T.; Kurokawa, K.; Kumihara, H.; Yamamoto, M.; Miyasaka, T.; Ito, Y.; Hirayama, R.; Inoue, T.; Kirii, Y.; Nishiwaki, E.; Ohmoto, H.; Maeda, Y.; Ishibishi, E.; Inouhe, Y.; Yoshino, K.; Kondo, H. New Type of Metalloproteinase Inhibitor: Design and Synthesis of New Phosphonamide-Based Hydroxamic Acid. Submitted for publication.

(11) *3D-QSAR in Drug Design. Theory, Methods and Applications*; Kubinyi, H., Ed.; ESCOM: Leiden (NL), 1993.

(12) *3D-QSAR in Drug Design. Volume 2. Ligand-Protein Interactions and Molecular Similarity*; Kubinyi, H., Folkers, G., Martin, Y. C., Eds.; Kluwer/ESCOM: Dordrecht (NL), 1997.

(13) *3D-QSAR in Drug Design. Volume 3. Recent Advances*; Kubinyi, H., Folkers, G., Martin, Y. C., Eds.; Kluwer/ESCOM: Dordrecht (NL), 1998.

(14) Cramer, R. D., III; Patterson, D. E.; Bunce, J. D. Comparative Molecular Field Analysis (CoMFA). 1. Effect of Shape on Binding of Steroids to Carrier Proteins. *J. Am. Chem. Soc.* **1988**, *110*, 5959−5967.

(15) Matter, H.; Schwab, W.; Barbier, D.; Billen, G.; Haase, B.; Neises, B.; Schudok, M.; Thorwart, W.; Schreuder, H.; Brachvogel, V.; Lönze, P.; Weithmann, K. U. Quantitative Structure−Activity Relationship of Human Neutrophil Collagenase (MMP-8) Inhibitors Using Comparative Molecular Field Analysis and X-ray Structure Analysis. *J. Med. Chem.* **1999**, *42*, 1908−1920.

(16) Matter, H.; Schwab, W. Affinity and Selectivity of Matrix Metalloproteinase Inhibitors: A Chemometrical Study from the Perspective of Ligands and Proteins. *J. Med. Chem.* **1999**, *42*, 4506−4523.

(17) Fichera, M.; Cruciani, G.; Bianchi, A.; Musumarra, G. A 3D-QSAR Study on the Structural Requirements for Binding to CB_1 and CB_2 Cannabinoid Receptors. *J. Med. Chem.* **2000**, *43*, 2300−2309.

(18) Martinez, A.; Gil, C.; Abasolo, M. I.; Castro, A.; Bruno, A. M.; Perez, C.; Prieto, C.; Otero, J. Benzothiadiazine Dioxide Dibenzyl Derivatives as Potent Human Cytomegalovirus Inhibitors: Synthesis and Comparative Molecular Field Analysis. *J. Med. Chem.* **2000**, *43*, 3218−3225.

(19) Gnerre, C.; Catto, M.; Leonetti, F.; Weber, P.; Carrupt, P.-A.; Altomare, C.; Carotti, A.; Testa, B. Inhibition of Monoamine Oxidases by Functionalized Coumarin Derivatives: Biological Activities, QSARs, and 3D-QSARs. *J. Med. Chem.* **2000**, *43*, 4747−4758.

(20) Pikul, S.; Dunham, K. L. M.; Almstead, N. G.; De, B.; Natchus, M. G.; Anastasio, M. V.; McPhail, S. J.; Snider, C. E.; Taiwo, Y. O.; Rydel, T.; Dunaway, C. M.; Gu, F.; Mieling, G. E. Discovery of Potent, Achiral Matrix Metalloproteinase Inhibitors. *J. Med. Chem.* **1998**, *41*, 3568−3571.

(21) Maskos, K.; Fernandez-Catalan, C.; Huber, R.; Bourenkov, G. P.; Bartunik, H.; Ellestad, G. A.; Reddy, P.; Wolfson, M. F.; Rauch, C. T.; Castner, B. J.; Davis, R.; Clarke, H. R. G.; Petersen, M.; Fitzner, J. N.; Cerretti, D. P.; March, C. J.; Paxton, R. J.; Black, R. A.; Bode, W. Crystal Structure of the Catalytic Domain of Human Tumor Necrosis Factor-α-converting Enzyme. *Proc. Natl. Acad. Sci. U.S.A.* **1998**, *95*, 3408−3412.

(22) Clark, M.; Cramer, R. D., III.; Van Opdenbosch, N. Validation of the general purpose Tripos 5.2 Force Field. *J. Comput. Chem.* **1989**, *10*, 982−1012, and SYBYL manual (SYBYL 6.6) including corrections to the Tripos 5.2 force field version.

(23) SYBYL 6.7. Tripos Assoc., 1699 S. Hanley Rd., St. Louis, MO 63144.

(24) Stewart, J. J. P. MOPAC 6.0, Quantum Chemical Program Exchange 455, 1990.

(25) Bohacek, R. S.; McMartin C. Definition and Display of Steric, Hydrophobic, and Hydrogen-Bonding Properties of Ligand Binding Sites in Proteins Using Lee and Richards Accessible Surface: Validation of a High-Resolution Graphical Tool for Drug Design. *J. Med. Chem.* **1992**, *35*, 1671−1684.

(26) Kellogg, G. E. Finding Optimum Field Models for 3D QSAR. *Med. Chem. Res.* **1997**, *7: 6/7*, 417−427.

(27) Bush, B. L.; Nachbar, R. B., Jr. Sample-distance Partial Least Squares: PLS optimized for many variables, with application to CoMFA. *J. Comput.-Aided Mol. Des.* **1993**, *7*, 587−619.

(28) Wold, S.; Albano, C.; Dunn, W. J.; Edlund, U.; Esbensen, K.; Geladi, P.; Hellberg, S.; Johansson, E.; Lindberg, W.; Sjostrom, M. In *Chemometrics: Mathematics and Statistics in Chemistry*; Kowalski, B., Ed.; Dordrecht, The Netherlands, 1984.

(29) Bursi, R.; Grootenhuis, P. D. J. Comparative molecular field analysis and energy interaction studies of thrombin-inhibitor complexes. *J. Comput.-Aided Mol. Des.* **1999**, *13*, 221−232.

JM0110385